A QM/MM Study of the Racemization of Vinylglycolate Catalyzed by Mandelate Racemase Enzyme

Mireia Garcia-Viloca, Àngels González-Lafont, and José M. Lluch*

Contribution from the Departament de Química, Universitat Autònoma de Barcelona, 08193 Bellaterra (Barcelona), Spain

Received August 3, 2000

Abstract: The experimentally postulated mechanism for the interconversion between (*S*)-vinylglycolate and (*R*)-vinylglycolate catalyzed by mandelate racemase enzyme consists of a two-step quite symmetric process through a dianionic enolic intermediate that is formed after the abstraction of the α-proton of vinylglycolate by a basic enzymatic residue and is then reprotonated by another residue. The challenging problem behind this reaction is how the enzyme manages to stabilize such an intermediate, that is, how it lowers enough the high pK_a of the α-proton for the reaction to take place. The QM/MM simulations performed in this paper indicate that catalysis is based on the stabilization of the negative charge developed on the substrate along the reaction. We have identified three different reaction mechanisms starting from different quasi-degenerate structures of the substrate−enzyme complex. In two of them the stabilizing role is done by means of a catalytic proton transfer that avoids the formation of a dianionic intermediate, and they involve six steps instead of the two experimentally proposed. On the contrary, the third mechanism passes through a dianionic species stabilized by the concerted approach of a protonated enzymatic residue during the proton abstraction. The potential energy barriers theoretically found along these mechanisms are qualitatively in good agreement with the experimental free energy barriers determined for racemization of vinylglycolate and mandelate. The theoretical study of the effect of the mutation of Glu317 by Gln317 in the kinetics of the reaction reveals the important role in the catalysis of the hydrogen bond formed by Glu317 in the native enzyme, as only one of the mechanisms, the slower one, is able to produce the racemization in the active site of the mutant. However, we have found that this hydrogen bond is not an LBHB within our model.

Introduction

Most enzymes, which are intrinsically asymmetric, are known to be impeccably stereoselective. Intriguingly, racemases (and their closely related epimerases) are able to process both substrate enantiomers (or diastereoisomers in the case of epimerases) with similar efficiency, thus suggesting that they have evolved some kind of pseudosymmetry in their active sites.[1]

One of the racemases for which an X-ray crystal structure has been resolved is mandelate racemase (including several of its mutational variants).[1] Its crystal structure shows that mandelate racemase is composed of two major structural domains (an N-terminal $\alpha + \beta$ domain and a central parallel α/β-barrel) and a third, smaller, irregular C-terminal domain. Mandelate Racemase (MR), the Enzyme Commission (EC) classification number of which is 5.1.2.2, belongs to the main class 5 of enzymes (isomerases). This enzyme catalyzes the reversible interconversion of the (*S*)- and (*R*)-enantiomers of mandelate (Figure 1). Mandelate racemase is part of the mandelate pathway in the soil bacteria *Pseudomonas putida*, which is composed of five enzymes that catalyze the conversion of the enantiomeric pair of mandelates to benzoate. Mandelate pathway, coupled to the so-called β-ketoadipate pathway, permits these bacteria to use either (*S*)- or (*R*)-mandelate as a sole source of carbon and energy.

Mandelate racemase is Mg^{2+}-dependent, and the racemization it catalyzes is supposed to be stepwise: it takes place through abstraction of the α-proton (that adjacent to the carboxylate group) from either enantiomer of mandelate, followed by stereorandom reprotonation of a transient enolic intermediate. A variety of mechanistic investigations based on isotope exchange and the site-directed mutagenesis experiments suggest that mandelate racemization proceeds by a two-base mechanism. In the active site of mandelate racemase the ϵ-amino group of Lys166 is the general base catalyst that abstracts the α-proton from (*S*)-mandelate, whereas the imidazole group of His297 acts as the general base catalyst that removes the α-proton from (*R*)-mandelate. The conjugate acids of Lys166 and His297 serve as the proton donors in the formation of (*S*)- and (*R*)-mandelate, respectively. Actually, this is the mechanism described by Kenyon et al. that is pictured in Figure 2.[1]

Figure 1. Reaction catalized by mandelate racemase enzyme.

However, a stepwise process through an enolic intermediate poses a challenging problem: how can mandelate racemase catalyze rapid proton exchange involving carbon−hydrogen bond cleavage of carbon acids with quite high pK_a values? In effect, the pK_a of the α-proton of mandelic acid has been measured to be 22.0, and the pK_a of the α-proton of mandelate anion has been estimated to be ∼29, while pK_a's of the conjugate acids of the general base catalysts Lys166 and His297 are

(1) Kenyon, G. L.; Gerlt, J. A.; Petsko, G. A.; Kozarich, J. W. *Acc. Chem. Res.* **1995**, *28*, 178.

10.1021/ja002879o CCC: $20.00
Published on Web 01/06/2001

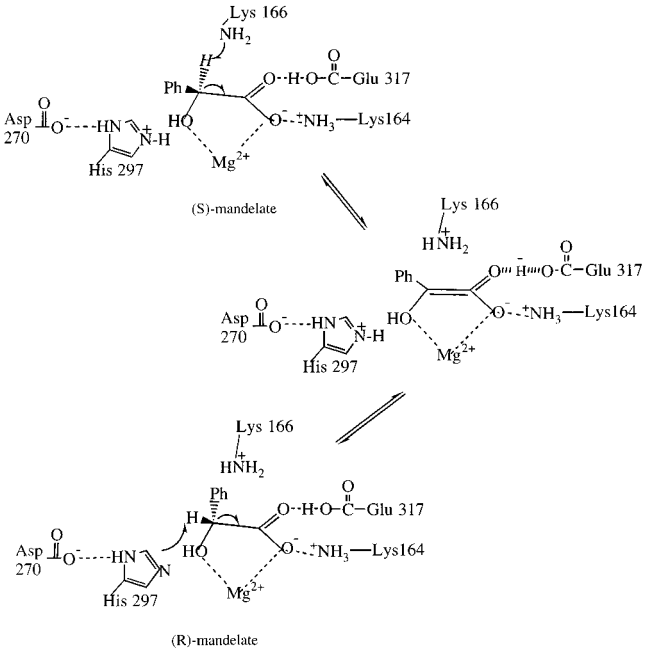

Figure 2. The proposed mechanism of ref 4 for the enzyme mandelate racemase.

thought to be ~6. Due to these very significant differences between the pK_a's of the substrate and the conjugate acids of the active-site general base catalysts the formation of the enolic intermediate should be a process thermodynamically (and, therefore, kinetically) quite unfavorable. In effect, sodium mandelate undergoes exchange of its α-proton in 0.40 M NaOD in D_2O only very slowly even at 100 °C.[1] Surprisingly, the measured k_{cat} for the racemization by mandelate racemase turns out to be as high as ~500 s^{-1} at 25 °C even at pH 7.5.[2] It has to be recalled that the constant k_{cat}, called the turnover number, is often applied to enzyme-catalyzed reactions: it represents the maximum number of substrate molecules (when the substrate concentration is very high) which can be converted to products per molecule of enzyme per unit time.[3]

That puzzling question is a general problem in enzymology that appears in the reactions catalyzed by many other enzymes, for example, triose-phosphate isomerase, Δ^5-ketosteroid isomerase, citrate synthase, enolase, aconitase, and fumarase.[4] In the last years some authors have suggested that the formation of a special kind of hydrogen bond, the so-called low-barrier hydrogen bond (LBHB), which would be largely covalent, can stabilize intermediates and transition states of enzymatic reactions.[5−7] In a monodimensional approach, according to the definition given by Cleland and Kreevoy,[5] a hydrogen bond can be defined as an LBHB if the ground vibrational level of the monodimensional double-well reaction path describing the proton jump lies at or above the classical energy barrier (i.e., without including zero-point energy) for the proton transfer. Nowadays, opposing viewpoints have led to an intense debate on the strength of an LBHB and its role in enzymatic catalysis.[8−21] So, Warshel et al.[9] have claimed that any transition-state stabilization attributed to an LBHB can probably be interpreted simply as electrostatic and that the formation of an LBHB would destabilize an enzyme transition state relative to water.

Interestingly, the experimental studies on the racemization catalyzed by mandelate racemase provided the basis for the early statements of the proposal that LBHBs are important in enzymatic catalysis. The analysis of the X-ray crystal structure of a complex of mandelate racemase with the competitive inhibitor (*S*)-atrolactate (that is, (*S*)-α-methylmandelate) reveals that one carboxylate oxygen of the bound inhibitor, and, by analogy, the substrate mandelate, is coordinated to the essential Mg^{2+} and also hydrogen-bonded to the ϵ-ammonium group of Lys164.[1] Gerlt and Gassman proposed that these interactions allow the bound mandelate anion to resemble bound mandelic acid electronically, this way, as mentioned above, reducing the pK_a of the α-proton of the substrate from 29 to 22.[4] Since this last value is still too high, Gerlt and Gassman suggested that the transition state and the enolic intermediate are stabilized due to the formation of an LBHB between the other carboxylate oxygen of the substrate and a general acid catalyst, Glu317. However, no evidence for this has ever been presented. As a matter of fact, the complex with (*S*)-atrolactate shows that the corresponding O−O distance is ~2.7 Å. This value indicates that Glu317 is protonated when substrate binds to the active site,[1,4] but it rather corresponds to a normal hydrogen bond.

To test the importance of Glu317 in the reaction catalyzed by mandelate racemase, the glutamic acid was mutated to a glutamine to generate the E317Q mutant. A comparison of the active-site structures for wild-type mandelate racemase and E317Q complexed with (*S*)-atrolactate revealed that no detectable differences in active-site geometry result from the substitution of a carboxylic group by a carboxamide group at residue 317. However, the k_{cat} values were reduced 4.5×10^3-fold for (*R*)-mandelate as substrate and 2.9×10^4 − fold for (*S*)-mandelate as substrate, so confirming the important role of Glu317 during the catalytic process.[2]

A theoretical study would be required in order to complement the experimental results and to provide a detailed picture of the molecular mechanism of the racemization. However, to our knowledge, only an ab initio study using a model system as simple as NH_3-mandelate-NH_4^+ has been carried out, giving a quite high energy barrier.[22]

The general purpose of this paper is to perform a realistic quantum mechanical/molecular mechanical (QM/MM) study of

(2) Mitra, B.; Kallarakal, A. T.; Kozarich, J. W.; Gerlt, J. A. *Biochemistry* **1995**, *34*, 2777.
(3) Palmer, T. *Understanding Enzymes*, 3rd ed.; E. Korwood: London, 1991.
(4) Gerlt, J. A.; Gassman, P. G. *J. Am. Chem. Soc.* **1993**, *115*, 11552.
(5) Cleland, W. W.; Kreevoy, M. M. *Science* **1994**, *264*, 1887.
(6) Gerlt, J. A.; Kreevoy, M. M.; Cleland, W.W.; Frey, P. A. *Chem. Biol.* **1997**, *4*, 259.
(7) Cleland, W. W.; Frey, P. A.; Gerlt, J. A. *J. Biol. Chem.* **1998**, *273*, 25529.
(8) Usher, K. C.; Remington, S. J.; Martin, D. P.; Drueckhammer, D. G. *Biochemistry* **1994**, *33*, 7753.
(9) Warshel, A.; Papazyan, A.; Kollman, P. A. *Science* **1995**, *269*, 102.
(10) Schwartz, B.; Drueckhammer, D. G. *J. Am. Chem. Soc.* **1995**, *117*, 11902.
(11) Scheiner, S.; Kar, T. *J. Am. Chem. Soc.* **1995**, *117*, 6970.
(12) Warshel, A.; Papazyan, A. *Proc. Natl. Acad. Sci. U.S.A.* **1996**, *93*, 13665.
(13) Shan, S.-O.; Herschlag, D. *Proc. Natl. Acad. Sci. U.S.A.* **1996**, *93*, 14474.
(14) Guthrie, J. P. *Chem. Biol.* **1996**, *3*, 164.
(15) Garcia-Viloca, M.; González-Lafont, A.; Lluch, J. M. *J. Am. Chem. Soc.* **1997**, *119*, 1081.
(16) Garcia-Viloca, M.; Gelabert, R.; González-Lafont, A.; Moreno, M.; Lluch, J. M. *J. Am. Chem. Soc.* **1998**, *120*, 10203.
(17) Ash, E. L.; Sudmeier, J. L.; De Fabo, E. C.; Bachovchin, W. W. *Science* **1997**, *278*, 1128.
(18) Pan, Y.; McAllister, M. A. *J. Am. Chem. Soc.* **1997**, *119*, 7561.
(19) McAllister, M. A. *Can. J. Chem.* **1997**, *75*, 1195.
(20) Kato, Y.; Toledo, L. M.; Rebek, J., Jr. *J. Am. Chem. Soc.* **1996**, *118*, 8575.
(21) Perrin, L. C.; Nielson, J. B. *Annu. Rev. Phys. Chem.* **1997**, *48*, 511.
(22) Alagona, G.; Caterina, G.; Kollman, P. A. *J. Mol. Struct.* **1997**, *390*, 217.

the mechanism of the reaction catalyzed by mandelate racemase. As specific objectives we will investigate if the racemization is as simple as that postulated from the experimental results (one step from (*S*)-mandelate to the enolic intermediate and a second step from this to (*R*)-mandelate), the role of the most important residues that lie in the active center (specially Glu317), and the possible existence and effect of whatever LBHB. To reduce the computational effort we have concretely studied the racemization of vinylglycolate (that includes an α-vinyl group instead of an α-phenyl group as in mandelate) which has also been found to be an excellent substrate of mandelate racemase.[23]

Methods and Calculation Details

The combined QM/MM potential implemented in AMBER 5.0[24] (Roar-cp module) was applied to model the reaction. The Roar-cp[25] module is the result of coupling together SANDER, the basic energy minimizer and molecular dynamics program of AMBER, and the semiempirical quantum mechanical program Mopac 7.0.[26] In the QM/MM technique a small region at the active site of an enzyme is described quantum mechanically, whereas the surrounding protein is included by a simpler MM representation. The QM atoms are influenced by the partial charges of the MM atoms, and in addition, bonded and van der Waals interactions between the two regions are included consistently. This method has been used successfully to model a few enzyme reactions and also reactions in solution. We have used link atoms to cap exposed valence sites due to bonds which cross the QM/MM boundary.[27]

Choice of the QM level and the MM Force Field. The QM part of the system is represented at the semiempirical MO level. Many of the computational studies on enzyme reactions (besides the very relevant Warshel's EVB studies[9,12]) have been done successfully using the AM1 parametrization.[28−33] In general, the accuracy of the AM1 method is assessed by comparison with ab initio results, and it leads to the conclusion that there is good agreement between the determined ab initio and AM1 geometries. However, the AM1 barrier heights are found to be overestimated in many cases.[28,31−33] Fewer studies on biological systems have been done at the PM3 semiempirical MO level, but these also have demonstrated the adequacy of the PM3 parametrization.[34−36] In this work, test calculations on a small model of the reaction under study have been done in order to determine the best choice between AM1 and PM3 semiempirical MO levels, by comparison with DFT results. Concretely, we have calculated the energy profile for abstraction of the α-proton of vinylglycolate substrate by an ethylamine that models the residue Lys166 in the active site of mandelate racemase enzyme. There is no stable product at the end of the reaction coordinate for any AM1, PM3, or B3LYP/6-31+G(d,p) levels. That is, the reaction is not possible in gas phase. However, the comparison between the geometries and energies found along the reaction profiles of each method allowed us to identify the PM3 method as the best choice in this case. The AM1 results indicated higher relative energies between reactants and different points along the energy profiles and a worse description of the hydrogen bonds. The QM part of the model used contains a Mg ion coordinated to six ligands. The X-ray crystal structure of a complex of mandelate racemase with the competitive inhibitor (*S*)-atrolactate indicates that the distance between the Mg ion and the oxygen atoms of the ligands is within the range 2.0−2.5 Å. However, our preliminary results using the PM3 parametrization for Mg indicate shorter distances, with deviations of 0.2−0.6 Å from the experimentally determined distances. The test set of molecules with experimentally known data that has been used to develop the Mg parameters for the PM3 Hamiltonian consisted basically of the magnesium halide and other very small inorganic compounds.[37] That test set did not include data for larger molecules and compounds where magnesium is coordinated in quadratic planar, pentagonal pyramidal, and octahedral complexes. Then, Hutter et al.[38] have developed new AM1 parameters for magnesium using a genetic algorithm as optimization technique and including a wide variety of biologically relevant molecules that contain magnesium atoms with different coordinations. The use of these AM1 parameters for Mg ion improves a lot our geometrical results (the calculated distances are now between the experimental range 2.0−2.5 Å).

On the other hand, we have used the AMBER force field by Weiner et al.[39] to describe the MM part of the system and the QM/MM van der Waals and electrostatic interactions.

The Model Used. The starting point for the calculations was the 2.0 Å resolution structure of the complex of *Pseudomas putida* mandelate racemase enzyme inactivated with (*R*)-α-phenylglycidate (Protein Data Bank code 1MNS).[40] For meaningful calculations to be performed, it is essential that a high-resolution structure is used and that this accurately represents the enzyme−substrate complex. (*R*)-α-PGA corresponds in absolute configuration to (*S*)-mandelate and cleanly forms a covalent adduct with the ϵ-amino group of Lys166. Experimentally it has been demonstrated that both inhibitors, (*S*)-atrolactate and (*R*)-α-PGA, bind wild-type MR exactly in the manner in which (*S*)-mandelate binds K166R mutant.[1] Therefore, the chosen structure should serve as a good model of the reactive complex.

From this crystallographic structure we have taken the Cartesian coordinates of the 2700 atoms that belong to enzyme residues, and we have discarded the coordinates corresponding to the 209 crystallographic waters, with the exception of the water directly bound to the metal Mg ion in the active center. Instead of keeping the crystallographic waters, we have solvated the active center with a sphere of TIP3P water molecules of radius 20 Å, centered on the magnesium atom, that is, 202 water molecules that are submitted to a soft harmonic potential to prevent their moving away from the active center. We have substituted the (*R*)-α-PGA inhibitor found in the X-ray structure by the (*S*)-vinylglycolate molecule, superimposing as many atoms as possible. As said previously, vinylglycolate is an excellent substrate of mandelate.[23] To evaluate from an energetically point of view the differences between mandelate and vinylglycolate substrates in the reaction catalyzed by MR enzyme, we have calculated at the B3LYP[41] level the energy required for the gas-phase abstraction of the α-proton in the three following molecules: glycolate (516 kcal/mol), (*S*)-vinylglycolate (481 kcal/mol), and (*S*)-mandelate (469 kcal/mol). The smallest classical energy for the gas-phase abstraction corresponds to mandelate,

(23) Li, R.; Powers, V. M.; Kozarich, J. W.; Kenyon, G. L. *J. Org. Chem.* **1995**, *60*, 3347.
(24) Pearlman, D. A.; Case, D. A.; Caldwell, J. W.; Ross, W. S.; Cheatham, T. E.; DeBolt, S.; Ferguson, D.; Seibel, G.; Kollman, P. A. *Comput. Phys. Com.* **1995**, *91*, 1.
(25) Cheng, A.; Stanton, R. S.; Vincent, J. J.; van der Vaart, A.; Damodaran, K. V.; Dixon, S. L.; Hartsough, D. S.; Mori, M.; Best, S. A.; Monard, G.; Garcia-Viloca, M.; Van Zant, L. C. and Merz, K. M., Jr. *ROAR 2.0*, The Pennsylvania State University, 1999.
(26) Stewart, J. J. P. MOPAC: A General Molecular Orbital Package. *Quantum Chem. Prog. Exch.* **1990**, *10*, 86.
(27) (a) Warshel, A.; Levitt, M. *J. Mol. Biol.* **1976**, *103*, 227. (b) Field, M. J.; Bash, P. A. Karplus, M. J. *J. Comput. Chem.* **1990**, *11*, 700. (c) Monard, G.; Merz, K. M., Jr. *Acc. Chem. Res.* **1999**, *32*, 904.
(28) Mullholand, A. J.; Richards, W. G. *Proteins* **1997**, *27*, 9.
(29) Cunningham, M. A.; Ho, L. L.; Nguyen, D. T.; Gillilan, R. E.; Bash, P. A. *Biochemistry* **1997**, *36*, 4800.
(30) Mulholland, A. J.; Richards, W. G. *J. Phys. Chem. B* **1998**, *102*, 6635.
(31) Ridder, L.; Mulholland, A. J.; Vervoort, J.; Rietjens, I. M. C. M. *J. Am. Chem. Soc*. **1998**, *120*, 7641.
(32) Antonczak, S.; Monard, G.; Ruiz-López, M. F.; Rivail, J.-L. *J. Am. Chem. Soc.* **1998**, *120*, 8825.
(33) Turner, A. J.; Moliner, V.; Williams, I. H. *Phys. Chem. Chem. Phys.* **1999**, *1*, 1323.
(34) Andrés, J.; Moliner, V.; Krechl, J.; Silla, E. *J. Chem. Soc. Perkin Trans.* **1995**, *2*, 1551.
(35) Merz, K. M., Jr.; Banci, L. *J. Phys. Chem.* **1996**, *100*, 17414.
(36) Burton, N. A.; Harrison, M. J.; Hart, J. C.; Hillier, I. H.; Sheppard, D. W. *Faraday Discuss.* **1998**, *110*, 463.
(37) Stewart, J. J. P. *J. Comput. Chem.* **1991**, *12*, 320.
(38) Hutter, M. C.; Hughes, J. M.; Reimers, J. R.; Hush, N. S. *J. Phys. Chem. B* **1999**, *103*, 4906.
(39) Weiner, S. J.; Kollman, P. A.; Case, D. A.; Singh, U. C., Ghio, C.; Alagona, G.; Profeta, S., Jr.; Weiner, P. *J. Am. Chem. Soc.* **1984**, *106*, 765.
(40) Landro, J. A.; Gerlt, J. A.; Kozarich, J. W. *Biochemistry* **1994**, *33*, 635.
(41) (a) Becke, A. D. *J. Chem. Phys.* **1993**, *98*, 5648. (b) Becke, A. D. *J. Chem. Phys.* **1996**, *104*, 1040. (c) Becke, A. D. In *Modern Electronic Structure Theory*; Yarkony, D. R.; Ed.; World Scientific: Singapore, 1995.

Table 1. Composition of the Quantum System of Three Models of the Complex MR-substrate[a]

	residues	heavy at./R	*q* link	*q* total	*q* Mg
model 1	Lys166	4	0.32	−2	0.55
	Asp195	4	0.68		
	Glu221	4	0.48		
	Glu247	4	0.38		
	Glu317	4	0.38		
	substrate	7	−		
	Mg	1	−		
	H_2O	1	−		
model 2	Lys166	5	−0.17	1	1.26
	Glu317	5	−0.01		
	substrate	7	−		
	Mg	1	−		
model 3	Lys164	3	0.04	0	0.56
	Lys166	4	0.00		
	Asp195	4	0.13		
	Glu221	4	0.04		
	Glu247	5	−0.06		
	His297	5	−0.01		
	Glu317	4	0.01		
	substrate	7	−		
	Mg	1	−		
	H_2O	1	−		

[a] The second column indicates the number of heavy atoms that are represented quantum mechanically in each residue. It contains also the Mulliken charges of the link atoms, *q* link, the total charge of the quantum system, *q* total, and the metal charge, *q* Mg, in au

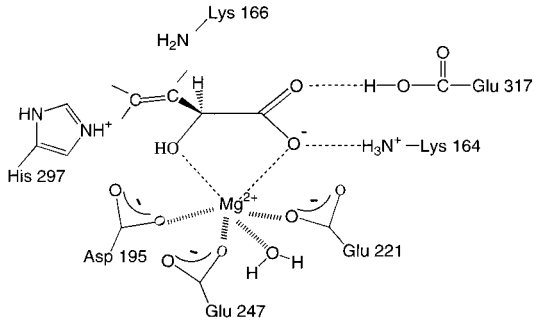

Figure 3. Scheme of the active center of the enzyme mandelate racemase bounded with (*S*)-vinylglycolate.

but vinylglycolate energy is closer to this smallest value than to the higher-energy value obtained for glycolate. Our results also show that the vinyl substitute is able to stabilize the increase in negative charge that accompanies the abstraction in a manner similar to that of the phenyl, as indicated by the comparison between the electronic charge distribution in vinylglycolate and mandelate dianions.

We have added the hydrogen atoms that were not determined by the crystallographic technique using the EDIT module of AMBER,[24] but we did not represent explicitly all of the hydrogen atoms because we used AMBER united atom model for the enzymatic residues that belong to the MM part of the system. The protein complex has been neutralized by placing four Na^+ in positions of large positive electrostatic potential and far enough of the active center.

In addition to magnesium ion and substrate (*S*)-vinylglycolate, we had to choose which residues we wanted to partially represent quantum mechanically and where we wanted to place the QM/MM frontier in each of them. We built three models of the enzymatic system with a different QM/MM partition, that can be understood by looking at Table 1 and Figure 3. For the three cases, to preserve integral charge in the MM region, the partial charges of the first MM $-CH_2$ group in each partially modeled residue were changed.[35] In model 1 the QM system has a total charge of −2 atomic units, and it is formed by the side chains of all of the magnesium ligands and the Lys166 residue, that is the base that abstracts the α-proton in the S→R direction. As a consequence of the charge transfer from the ligands to the metal, the Mulliken charge of magnesium ion in this model is quite reduced (see Table 1). However, the charges of the link atoms indicate arbitrary polarization for the QM subsystem, probably caused for the exclusion of the Coulombic interactions between the link atoms and the MM atoms in the QM Hamiltonian.[42] The link atom charges should have magnitudes from 0 to ±0.2 au, and they can be reduced by increasing the size of the QM portion of the residue traversing the QM/MM frontier. In this sense we built model 2, where the QM part of residues Lys166 and Glu317 is larger. We also discarded from the QM subsystem the water directly coordinated to the metal and the three negatively charged Mg ligands to decrease the negative charge in the QM system. Table 1 shows that there are no unrealistically large partial charges on the hydrogen link atoms. This result seems to indicate that the extra negative charge in the QM subsystem might also cause the arbitrary polarization. However, model 2 is not completely adequate as magnesium density charge is not well represented, because charge transfer from its ligands is not feasible. The comparison between the magnesium Mulliken charges obtained for each model supports this idea. As a consequence, we decided to build model 3 in which the QM subsystem is equal to the one in model 1, but we have added two enzymatic residues with positive charge, Lys164 and His297, to reduce the negative charge of the quantum system. In addition, it was necessary to lengthen the quantum part of Glu247 residue. The magnesium and the link atom partial charges in this model indicate that there is a good distribution of charge density in the QM system. As a consequence, model 3 was chosen to be used in the following calculations. This model contains 3957 atoms, and 75 of them are QM atoms.

From this model of the complex formed between MR wild-type enzyme and (*S*)-vinylglycolate we built the model of the reactive complex between E317Q mutant and (*S*)-vinylglycolate, by replacing the $-COOH$ group of the side chain of residue 317 with a $-CONH_2$ group. In this way, the theoretical results obtained for the wild-type enzyme and the E317Q mutant are directly comparable.

QM/MM Calculations. Minimizations and Molecular Dynamics Simulations. QM/MM potential energy optimizations have been carried out taking into account all of the interactions; that is, no cutoff was applied for the nonbonded interactions. A 15 Å sphere was defined around the active-site magnesium atom, and only residues within this sphere as well as the water molecules were allowed to move during the simulations that result in 1293 moving atoms. Starting from the model structure of the reactive complex in both wild-type and mutant active sites, the QM/MM potential energy was minimized until the root-mean square (rms) gradient fell bellow 0.001 kcal/(molÅ), by means of the L-BFGS method.[43] The resultant stationary points were taken as the reference structure that models the reactant of the S→R reaction, for MR wild-type or E317Q mutant active centers, respectively. From each reference structure we have calculated the energy profiles of different possible mechanisms of the enzymatic reactions. We have minimized the QM/MM potential energy along a suitable reaction coordinate for each of the transformations, with the convergence criterion described above. Concretely, the distance between the acceptor atom and the hydrogen that is being transferred in each step is taken as reaction coordinate, and a harmonic potential is applied on this distance: $V = K(r - r_{eq})^2$, where r_{eq} defines every point of the corresponding energy profile and $K = 10\,000$ kcal/(mol·Å^2).

Calculating reaction paths for chemical or conformational changes in enzymes is a challenging problem because of the large size of the system. This presents difficulties both computationally, in characterizing true transition-state structures (TSs) and their associated pathways, and because of the complex nature of protein potential energy surfaces. In this work, TS stands for the structure of maximum classical potential energy at every step of the mechanism. At the moment, the Roar-2.0 program does not have the adequate algorithm for direct location of transition state structures.[25] On the other hand, taking into account that the energy minimization techniques are prone to being trapped in local minima that are near the initial starting structure, we have carried out QM/MM molecular dynamics simulations in the *NVT* ensemble (number of particles, volume, and temperature are fixed). Then, new possible structures that represent the reactant and the product complexes

(42) Gao, J.; Amara, P.; Alhambra, C.; Field, M. J. *J. Phys. Chem. A* **1998**, *102*, 4714.
(43) Liu, D. C.; Nocedal, J. *Math. Programming* **1989**, *45*, 503.

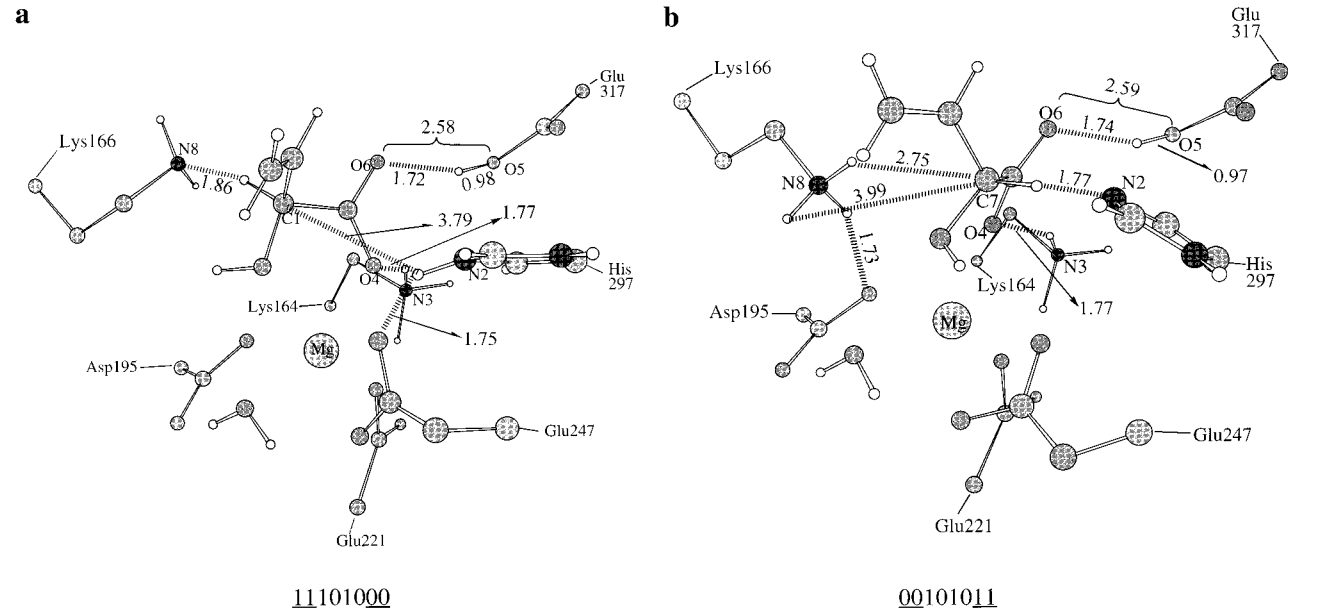

Figure 4. (a) Structure of the active site at the stationary point S. The labels used correspond to the following atoms: C1, α-carbon of (*S*)-vinylglycolate enantiomer; N2, ϵ-nitrogen of His297; N3, amino nitrogen of Lys164; O4, oxygen of the carboxylate group of the substrate; O5, oxygen of the carboxylic group of Glu317; O6, oxygen of the carboxylate group of the substrate; N8, amino nitrogen of Lys166. Distances are given in Å. (b) Structure of the active site at the stationary point R. The labels used to identify some atoms are the same as in (a), with the exception of C7, that corresponds to the α-carbon of (*R*)-vinylglycolate enantiomer. Distances are given in Å.

formed by (*S*)-vinylglycolate or (*R*)-vinylglycolate, respectively, complexed with the enzyme can be found. The following calculations were performed for both complexes. Starting from the minimized complex, a QM/MM molecular dynamics simulation was performed with 1 fs time step to heat the system from 0 to 300 K over an interval of 6 ps, with atom velocities assigned from a Gaussian distribution every 2 ps in 100 K increments. The system was equilibrated for an additional 10 ps run. The temperature was maintained by coupling to two thermostat chains (one for the MM region and the other for the QM region) within the Nosé−Hoover chain temperature scheme.[44] We have used three thermostats for each chain, and the program has automatically set the mass values of each of them. The nonbond cutoff distance was 10 Å for the MM atoms, whereas we used a distance of 100 Å, that is, noncutoff, for the QM atoms. The reason of doing so is based on the high dependence of the energy of the QM portion on the cutoff used. The nonbond pair list was updated every 25 steps, and the SHAKE algorithm[45] was used to constrain bond distances that imply hydrogen atoms.

Results and Discussion

Starting from the model structure of the complex formed between (*S*)-vinylglycolate and mandelate racemase enzyme, the optimization of the moving part of the system leads to the minimum energy structure that is partially represented in Figure 4a and that we have called structure S. The labels used in Figure 4a to identify some of the atoms will be used throughout and correspond to atoms located in eight positions that are able to be occupied or unoccupied by means of proton-transfer processes, as we will describe later. The short distance (1.86 Å) between the amino nitrogen of Lys166 residue (N8 in Figure 4a) and the α-proton attached to the C1 atom of the substrate is consistent with the basic catalytic role that has been attributed to this residue in the S-to-R direction.[1] That is, this geometry is ready for facile transfer of a proton between substrate and the functional group of Lys166. On the contrary, His297 residue is further from the α-carbon (3.79 Å), because of its interaction with the carboxylate group of Glu247 by means of the formation of a hydrogen bond. This result is in agreement with the X- ray determined value of 3.8 Å for the distance between the α-carbon of (*R*)-α-phenylglycidate and the ϵ-nitrogen of His297.[46] On the other hand, the minimization of the QM/MM potential energy starting from the model structure of the complex between (*R*)-vinylglycolate and mandelate racemase enzyme (that only differs from the previous model structure in the substrate configuration) leads to the minimum energy structure partially represented in Figure 4b (structure R). Contrary to the structure S, the deprotonated ϵ-nitrogen of His297 is oriented to the α-proton attached to the C1 carbon, as it is expected if His297 is the basic catalyst in the R-to-S direction. In addition, we can observe how the conjugate acid of Lys166 has moved further from the α-carbon with respect to its position in the structure S, and it is interacting with another magnesium ligand by hydrogen bonding. At this point it is worthy to note that we are not able to directly compare the theoretically determined structure R with any X- ray structure of MR enzyme bounded to an analogous of the (*R*)-enantiomer of the substrate. While the structures of (*S*)-atrolactate and (*R*)-α-PGA bound to the racemase provide mechanistically valuable insight into the geometry of the interaction of the (*S*)-enantiomer of the substrate with functional groups in the active site, (*S*)-α-PGA fails to form a covalent adduct with MR, and (*R*)-atrolactate fails to bind in a unique geometry to the active site.[40] However, Landro et al.[40] have suggested that the mode of interaction of (*R*)-mandelate is similar to that encountered for (*S*)-mandelate. The six first rows of Table 2 contain the distances between the Mg cation and its ligands (vinylglycolate, Asp195, Glu221, Glu247, and a water molecule) in the active site of the theoretically (S and R) or experimentally[40] (exp) determined structures, that correspond to the MR enzyme complexed to (*S*)- and (*R*)-vinylglycolate or (*R*)-α-phenylglicidate, respectively (we will refer later to the second column of Table 2). The differences between the theoretical and the X-ray distances are very small,

(44) Cheng, A.; Merz, K. M., Jr. *J. Phys. Chem.* **1996**, *100*, 1927.
(45) van Gunsteren, W. F.; Berendsen, H. J. C. *Mol. Phys.* **1977**, *34*, 1311.
(46) Kallarakal, A. T.; Mitra, B.; Kozarich, J. W.; Gerlt, J. A.; Clifton, J. G.; Petsko, G. A.; Kenyon, G. L. *Biochemistry* **1995**, *34*, 2788.

Table 2. Distances (in Å) between Residues, and Charge of the Metal Ion (in au) in the Active Center of the Stationary Points S, S2, and R, and in the X-ray Structure (exp)

	S	S2	R	exp[a]
Mg−OH	2.26	2.27	2.39	2.28
Mg−O4	2.12	2.13	2.10	2.10
Mg−O(Asp195)	2.10	2.10	2.12	2.00
Mg−O(Glu221)	2.09	2.08	2.06	2.05
Mg−O(Glu247)	2.22/2.20	2.16/2.25	2.17/2.14	2.04
Mg−OHO	2.18	2.19	2.23	2.11
qMg	0.89	0.87	0.98	−
N3−O4	2.70	2.70	2.69	2.76
O5−O6	2.58	2.64	2.59	2.68

[a] PDB crystal structure with code number 1MNS.

and in fact, they might be a consequence of the different substrates bounded to the enzyme. However, it has to be pointed out that one of the magnesium ligands, Glu247 residue, which in the X-ray structure has only one of its carboxylic oxygens bound to the metal ion, changes this coordination along the minimizations that lead to the structures S and R to form two longer bonds with magnesium, one with each of its carboxylic oxygens. The last two rows of Table 2 show the theoretical and experimental distances between the heavy atoms involved in the hydrogen bonds formed between the carboxylic oxygens of the substrate and residues Lys164 and Glu317. The calculated distances are shorter than the experimentally determined ones, but they are comparable. On the other hand, we have also calculated the metal charge in the active site of our model, together with the charge of the rest of the quantum atoms. These partial charges have been derived from the quantum mechanical (PM3) electrostatic potential (ESP), by means of a least-squares fit between the model and the quantum mechanical potential in the active site, that is, under the influence of the MM system on the QM system. The seventh row of Table 2 indicates the metal charge in the active-site model. It turns out to be quite smaller than 2 au due to the charge transfer from the ligands to the metal. Although the Mulliken charge of Table 1 for Mg in the active site of model 3 (before optimization) is still smaller than the ESP values of Table 2, the two charge models show the same tendency that supports the quantum representation of Mg and its closer ligands to approach a good representation of the active center.

In addition, to further assess the goodness of the model, we have carried out QM/MM molecular dynamics simulations at 300 K starting from the minimized structures S and R, following the procedure described in the Methods and Calculation Details. In both cases the final active-site structure is geometrically comparable to the minimized one. This result brings us to the following conclusions: our model for the native enzyme is capable of generating stable MD simulations, and the possible active-site configurations with geometries very different from the one obtained with the minimizations are improbable.

Reaction Mechanism. Energy Profiles. From the minimized structure S (Figure 4a), that is, the reactant of our model of the racemization of vinylglycolate catalyzed by MR enzyme, we tried to locate the dianionic intermediate that should be formed when Lys166 abstracts the α-proton.We carried out a series of restrained minimizations, decreasing gradually the distance between the α-proton and the amino nitrogen of Lys166, from the 1.86 Å value that corresponds to the reactant (Figure 4a) to a distance of 1.00 Å, that would roughly correspond to the product of the proton transfer if it would exist. However, we did not manage to locate a stable product for this proton abstraction; that is, the QM/MM potential energy increases continually along this energy profile, and when we unfroze the fixed distance, the minimization led again to the minimum structure S. Moreover, we observe that along this abstraction the protonated His297 residue has not approached to the α-carbon from the (*R*)-face of the substrate.We suggest that the formation of a hydrogen bond between His297 and Glu247 prevents the approach of that protonated residue that otherwise would stabilize the negative charge of the dianionic substrate. We arrived at the same results by carrying out QM/MM molecular dynamics simulations constrained to a distance N8-α-proton equal to 1.0 Å, followed by unconstrained MD simulations.

Up to this point our results seemed to indicate that within our model the dianionic intermediate does not exist, probably as a consequence of the high negative charge developed on the substrate and the failure of the enzymatic residues to stabilize it. Then, we took into account two possible processes that would generate an anionic instead of a dianionic intermediate after the abstraction of the α-proton: the suggested proton transfer from the ϵ-ammonium group of Lys164 to the enolic intermediate or the possible proton transfer through the hydrogen bond between Glu317 and the other carboxylic oxygen of the substrate.[1,21] These proton transfers could give rise to two different mechanisms that lead from (*S*)-vinylglycolate to an anionic intermediate, each one requiring a previous "catalytic" proton transfer, from Lys164 or from Glu317 to a carboxylic oxygen of the substrate, respectively. Effectively, we found two minima that are partially represented in Figure 5 and that we have called structures I2. They correspond to the anionic intermediates that result from the abstraction by Lys166 of the α-proton of vinylglycolic acid, that is the product of the previous proton transfer from Lys164 (Figure 5a) or from Glu317 (Figure 5b) to a carboxylate oxygen of (*S*)-vinylglycolate. The energetic results of our simulations discarded that any of these proton-transfer processes were concerted with the α-proton abstraction. From now, we will refer to the proton transfers through the hydrogen bonds between vinylglycolate and Lys164 or Glu317 as "catalytic" proton transfers. Through these two processes one of the two protons involved may occupy the position that corresponds to the bond with N3 or with O4 (see Figure 5), and the other may occupy the O5 or the O6 position. These are the positions 3, 4, 5, and 6, respectively, that we will call "catalytic" positions. On the other hand, the positions that correspond to the bond of the two participating protons with C1 or N8 and with C7 or N2 become occupied or unoccupied along what it is really the racemization reaction. As a consequence, the positions labeled with the numbers 1, 8, 7, and 2, respectively, will be the "reactive" positions. We should take into account that positions 1 and 7 are really the same, but when the hydrogen is attached to C1 or C7, it means that the proton comes from the (*S*)- or from the (*R*)-face, respectively. The stationary points S, R, and I2 can be defined by means of a binary code that describes the state in each of them of these eight positions that participate in proton-transfer processes. For example, if we assign the number 1 or 0 to a determinated position, to indicate that it is occupied or unoccupied, respectively, the structure S in Figure 4a has the code 11101000. That is, in this structure the reactive positions 1 and 2 and the catalytic positions 3 and 5 are occupied. We will use this binary code to define all of the different stationary points encountered along the reaction mechanisms that we will describe below. The reactive positions are always the first two and the last two of the code, they appear underlined, and in going from the complex between MR and the (*S*)-substrate to the complex with the (*R*)-substrate their states change from 11XXXX00 to 00XXXX11.

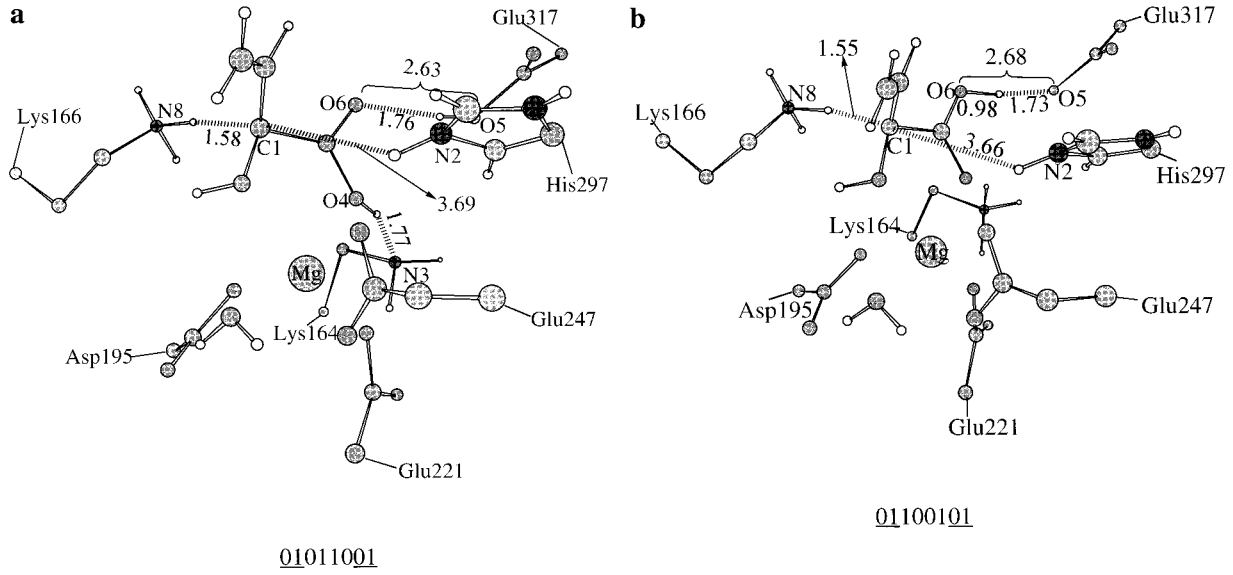

Figure 5. (a) Structure of the active site at the stationary point I2 for mec I. The labels used to identify some atoms are the same as in Figure 4. Distances are given in Å. (b) Structure of the active site at the stationary point I2 for mec II. The labels used to identify some atoms are the same as in Figure 4. Distances are given in Å.

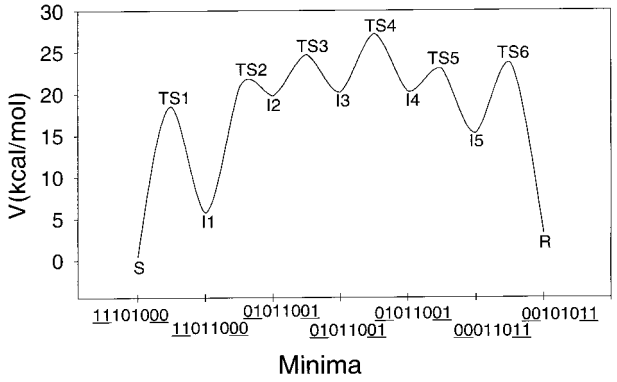

Figure 6. QM/MM potential energy profile of mec I. The numbers below the *x*-axis follow the code explained in the text to identify the different minimum energy structures found along the mechanism.

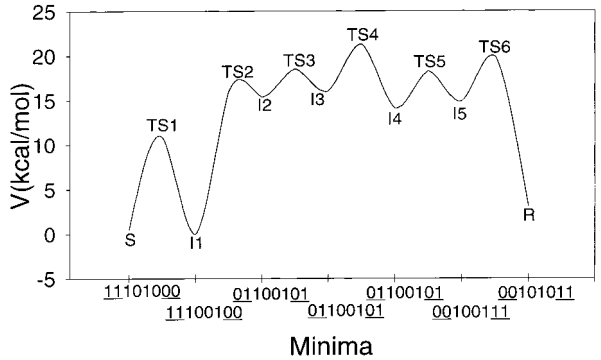

Figure 7. QM/MM potential energy profile of mec II. The numbers below the *x*-axis follow the code explained in the text to identify the different minimum energy structures found along the mechanism.

On the contrary, the four central positions are the catalytic ones; they do not appear underlined, and their initial and final states are the same in both racemization directions, from S to R or from R to S.

Figures 6 and 7 show the QM/MM energy profiles for the mechanisms that we have called mec I and mec II, which manage to racemize vinylglycolate via two catalytic steps that consist of the above-described proton transfers between the positions 3 and 4 or 5 and 6, respectively. The role of these catalytic steps in both racemization directions is to diminish the negative charge on the substrate along the reaction. Both mechanisms consist of six steps and are qualitatively very similar. Following the code on the abscissa axis of each profile it is seen that the first step of both mechanisms corresponds to a catalytic proton transfer, because there is a change in the binary numbers, from 10 to 01, of the central catalytic positions 3 and 4 for mec I or 5 and 6 for mec II, respectively. The result of this step in both mechanisms is the neutral substrate, that is vinylglycolic acid within our model. Similarly, the last step in both mechanisms is the catalytic process that returns the catalytic positions involved in each case to their initial state, via the same proton transfer as step 1 but in the opposite direction. The comparison of distance values along the first three rows of Tables 3 and 4, and the same comparison along the last three rows, indicate that during the catalytic steps 1 and 6, which in both mechanisms lead from the structure S to the intermediate I1 and from the intermediate I5 to the structure R, respectively, there are not important geometrical changes in the distances that involve reactive proton transfers. The results contained in the last column of Tables 3 and 4 show that the catalytic steps 1 and 6 are energetically less expensive for mec II than for mec I. In addition, the intermediate I1 in mec II is energetically quite degenerate with the reactant S, whereas I1 in mec I is

Table 3. Distances (in Å) between the Protons and the Heavy Atoms that Participate in Proton-Transfer Processes in the Different Stationary Points Found along Mec I and Potential Energy of Each Stationary Point

	C1−H	N8−H	C7−H	N2−H	*V* (kcal/mol)
S (11101000)	1.15	1.86	3.79	1.03	0.00
TS1	1.15	1.87	3.79	1.03	18.01
I1 (10011000)	1.16	1.83	3.84	1.03	6.13
TS2	1.56	1.24	3.68	1.03	20.27
I2 (01011001)	1.58	1.13	3.69	1.03	19.27
TS3	1.66	1.10	2.69	1.02	24.24
I3 (01011001)	1.62	1.11	2.97	0.99	19.71
TS4	2.43	1.01	1.89	1.03	26.72
I4 (01011001)	3.51	1.00	1.74	1.06	19.76
TS5	3.69	1.00	1.49	1.18	22.48
I5 (00011011)	3.79	1.00	1.19	1.74	14.79
TS6	3.41	1.00	1.18	1.75	23.23
R (00101011)	3.99	1.00	1.17	1.77	2.61

Table 4. Distances (in Å) between the Protons and the Heavy Atoms that Participate in Proton-Transfer Processes in the Different Stationary Points Found along Mec II and Potential Energy of Each Stationary Point

	C1−H	N8−H	C7−H	N2−H	*V* (kcal/mol)
S (11101000)	1.15	1.86	3.79	1.03	0.00
TS1	1.16	1.86	3.80	1.02	10.40
I1 (11100100)	1.16	1.84	3.82	1.02	−0.50
TS2	1.55	1.24	3.64	1.02	15.54
I2 (01100101)	1.55	1.16	3.66	1.02	14.89
TS3	1.62	1.12	2.89	1.02	18.08
I3 (01100101)	1.58	1.14	3.13	0.99	15.58
TS4	3.31	1.00	1.89	1.03	20.81
I4 (01100101)	3.44	1.00	1.84	1.04	13.63
TS5	3.87	1.00	1.39	1.54	17.80
I5 (00100111)	3.96	1.00	1.20	1.79	14.41
TS6	4.15	1.00	1.18	1.75	19.41
R (00101011)	3.99	1.00	1.17	1.77	2.61

higher in energy. Step 2 in both mechanisms corresponds to the abstraction of the α-proton attached to C1 by Lys166, that is the first reactive proton transfer of the racemization process and leads in each case to the anionic structures I2 represented in Figure 5. The fourth and fifth rows of Tables 3 and 4 show the geometrical parameters of the transition state (TS2) and the anionic intermediate I2 for mec I and the mec II, respectively. These geometrical parameters reproduce the movement of a proton from C1 carbon to N8 nitrogen in going from S to I2, and show that both structures TS2 are geometrically closer to the corresponding product I2 than to the reactant S, which is the expected behavior for an endothermic step. At this point, it is worthy to note that along step 2 of both mechanisms there has been only a very small change in the C7−H distance tabulated in the third column of Tables 3 and 4. That is, as said previously, the abstraction of the α-proton by Lys166 does not significantly alter the position of the catalytic residue His297, which is still very far from the C1 carbon in structures I2 (Figure 5). In addition, the α-carbon has not started to change its configuration in going from S to I2, that is, we are not able to label it as C7, that would correspond to the (*R*)-configuration, but it is not an sp2 carbon either. The last columns of Tables 3 and 4 indicate that in step 2, as in the case of step 1, both the QM/MM energy barrier and the resulting I2 intermediate, are higher in energy for mec I than for mec II.

Steps 3 and 4 do not correspond to any proton-transfer process, and for this reason the code that identifies the resulting intermediates, I3 and I4, is the same as for I2. The geometrical parameters of the TS structures for these steps turn out to be very similar to the parameters of the corresponding intermediates. The small energy barriers of these two steps are the result of small changes on the interactions where the residue that is the acid catalyst in the S-to-R direction (His297) participates. The reduction of the distance between the α-carbon and the proton attached to the ϵ-nitrogen of His297, C7−H in Tables 3 and 4, in going from I2 to I4, reflects the approach of this residue to the substrate. In the structure S, the ϵ-nitrogen N2 forms a hydrogen bond with Glu247 (see Figure 4a), and this interaction persists during steps 1 and 2, but it is broken during step 3, because the participating proton approaches to C7 (C7−H diminishes from 3.69 to 2.97 Å, or from 3.66 to 3.13 Å, in Table 3 or Table 4, respectively). As a consequence, the distance N2−H also diminishes for both mechanisms, because N2 loses its interaction with Glu247. In both mechanisms step 4 involves the energy maxima of the reaction path, which are the result of the configuration change of C1: from a configuration closer to that of the reactant S to a configuration similar to the one that corresponds to the product R, through an sp2 hybridation, that

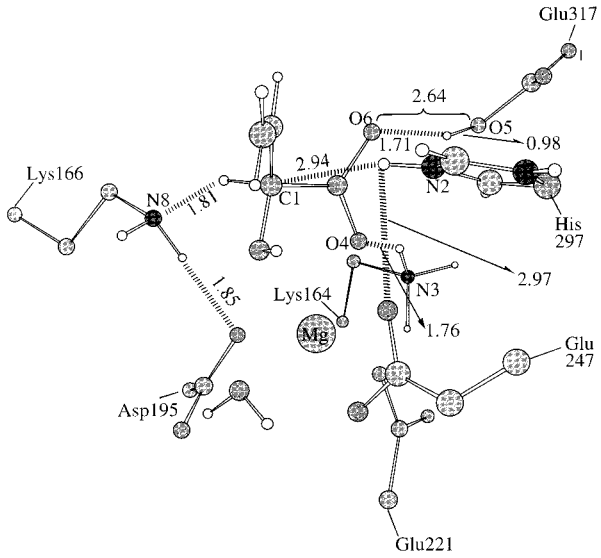

11101000

Figure 8. Structure of the active site at the stationary point S2. The labels used to identify some atoms are the same as in Figure 4. Distances are given in Å.

is, the change from C1 to C7 in our code in going from I3 to I4. The variation of the dihedral angle O6−C−C1(C7)−C_{vinyl}, that reflects the extent to which the configuration at C1 (or C7) inverts, illustrates the advance of the reaction: −59.1° (*S*), −30.1° (I3), 23.9° (I4), and 52.3° (*R*) for mec I; −59.1° (*S*), −27.7° (I3), 21.6° (I4), 52.3° (*R*) for mec II. This change from C1 to C7 is produced when His297 is close enough to the anionic intermediate to form an ionic pair with it (C7−H is 1.74 and 1.84 Å in I4 in Tables 3 and 4, respectively, and N2−H has become longer with respect to the previous intermediates). Step 5 is the reactive step that consists of the proton transfer from N2 to C7, through structure TS5. The final product R (Figure 4b) is accomplished in both mechanisms after the catalytic proton transfer during step 6, that returns the catalytic positions to their initial state.

Up to this point, we have found within our model two possible reaction paths that racemize vinylglycolate via an anionic intermediate. However, we wanted to reconsider the existence of a dianionic species along the reaction. From the structure S, the big distance between the protonated His297 and the substrate (Figure 4a) makes it difficult that this residue contributes to stabilize the dianionic intermediate after the α-proton abstraction by Lys166. As a consequence, the above explained catalytic proton transfers are required for the reaction to take place. However, a system with so many degrees of freedom is able to generate a lot of different configurations that can be rather degenerate in many cases. Then, we tried to find a structure that also models the reactive complex between MR and (*S*)-vinylglycolate, energetically and geometrically closer to S, but with the exception of His297 location, that we wanted to hold up closer to the monoanionic substrate to be prepared to stabilize the dianion. Taking S as the starting point, we failed to find such a structure. Likewise, no stable structure of the dianion has been found, despite forcing His297 to be closer to the carbanion by means of constrained minimizations. On the other hand, the observation of Figure 4b suggests that the R structure can be a good starting point to arrive to the reactive structure that we were looking for, as in this structure His297 is naturally located closer to the substrate. Effectively, we arrived to the structure S2, pictured in Figure 8, starting from the Cartesian

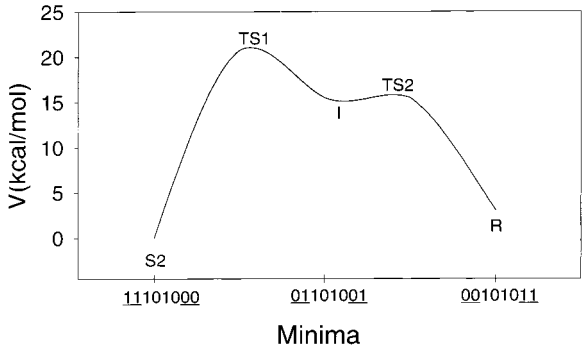

Figure 9. QM/MM potential energy profile of mec III. The numbers below the *x*-axis follow the code explained in the text to identify the different minimum energy structures found along the mechanism.

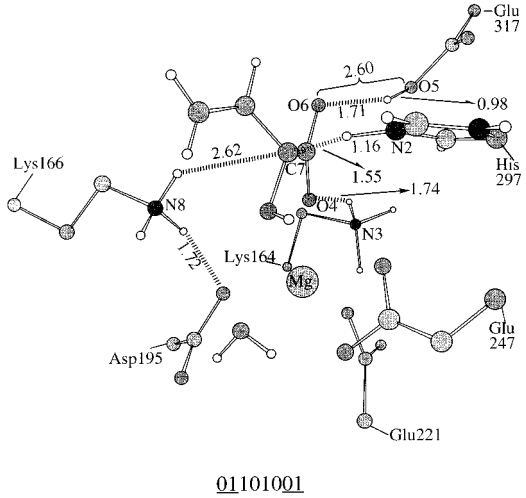

01101001

Figure 10. Structure of the active site at the stationary point I. The labels used to identify some atoms are the same as in Figure 4. Distances are given in Å.

coordinates of R but inverting the configuration of the α-carbon of the substrate. This structure is an alternative model of the reactive complex between MR and (*S*)-vinylglycolate, and it is 0.48 kcal/mol more stable than the structure S. The comparison between the two first columns of Table 2 indicates that S2 is also geometrically very close to S, with the exception of the distance (not included in Table 2) between the substrate and His297, that has reduced to 2.94 Å in S2 (Figure 8) with respect to the 3.79 Å value encountered in S (Figure 4a).

Figure 9 shows the QM/MM potential energy profile of the mechanism starting from S2 or R that racemizes vinylglycolate, without needing any previous catalytic proton transfer and via the dianionic intermediate I, that is partially represented in Figure 10. We have called this mechanism, mec III. The codes that identify the stationary points found along it only differ in the binary numbers that correspond to reactive positions and serve to indicate the reactive proton transfers that occur in going from S2 to I and from I to R. Table 5 resumes the geometric parameters and the energies related with these reactive proton transfers for the different stationary points of mec III.

A quick look to Figure 9 highlights that mec III is much simpler than both mec I and mec II, because it requires only two steps as it was proposed experimentally for this reaction. However, in opposition to the experimental conclusions it is a rather asymmetric mechanism.[4] Within our model this asymmetry is a consequence of the fact that the geometrical difference between S2 and I is greater than the geometrical difference between I and R. That is, the configuration of the α-carbon in

Table 5. Distances (in Å) between the Protons and the Heavy Atoms that Participate in Proton-Transfer Processes in the Different Stationary Points Found along Mec III and Potential Energy of Each Stationary Point

	C1−H	N8−H	C7−H	N2−H	*V* (kcal/mol)
S2 (11101000)	1.16	1.81	2.94	0.99	−0.48
TS1	2.02	1.03	1.76	1.07	20.28
I (01101001)	2.62	1.01	1.55	1.16	15.03
TS2	2.62	1.01	1.55	1.17	15.04
R (00101011)	2.75	1.01	1.17	1.77	2.61

Table 6. Comparison between the k_{cat} Determined Experimentally and the Free Energy Barriers, $\Delta G^{\ddagger}$ (in kcal/mol), Calculated from Them, with the Theoretical Potential Energy Barriers, $\Delta V^{\ddagger}$ (in kcal/mol)

	experimental $k_{cat}(s^{-1})$	results $\Delta G^{\ddagger}$	theoretical mec I	results: mec II	$\Delta V^{\ddagger}$ mec III
(*S*)-vinylglycolate	250 ± 20^a	14.27	26.72	20.81	20.76
(*S*)-mandelate	350 ± 5^b	14.07	−	−	−
(*R*)-vinylglycolate	240 ± 30^a	14.29	24.11	18.20	17.67
(*R*)-mandelate	500 ± 16^b	13.85	−	−	−

[a] From ref 23 [b] From ref 2

I is more similar to the one in R than to the corresponding one in S2. The values of the dihedral angle O6−C−C1(C7)−C_{vinyl} are −28.3° (S2), 41.3° (I), and 52.3° (R). For this reason we have labeled as C7 the α-carbon in the intermediate I (Figure 10). This configuration change implies that His297 approaches the α-carbon in going from S2 to I, until a distance similar to the one that corresponds to I4 in the other mechanisms (see distances C7−H for I4 in Tables 3 and 4 and for I in Table 5). That is, in going from S2 to I the α-carbon has to change its configuration in a concerted manner with the α-proton abstraction and the approach of His297. This result suggests why we did not manage to arrive at I from the structure S. In the structure S (Figure 4a) His297 forms a hydrogen bond with Glu247, that makes difficult the concerted changes described above, whereas on the contrary, this interaction does not exist in S2 (Figure 8). As a consequence, in mec I and mec II the stabilizing role of His297 is substituted by the required catalytic proton transfers from Lys164 and Glu317, respectively, and the α-proton abstraction does not imply the approach of His297 to the carbanion in I2 (see the distances C7−H in going from S to I2 in Tables 3 and 4). Indeed, mec III also stabilizes the dianionic intermediate I with hydrogen bonds from both Lys164 and Glu317. In opposition to the complicated set of motions involved along the step 1 in mec III, in going from I to R (step 2) only the delivery of a proton from His297 to the α-carbon occurs. In summary, we have explained why the energetic cost to go from S2 to I is quite higher than from R to I and why, as Table 5 indicates, the structure TS1 is geometrically closer to I, the product of the endoergic step 1, and structure TS2 is closer to the reactant of the exoergic step 2, that results to be the same intermediate I.

Let us now analyze our results from an energetic point of view. Table 6 allow us to compare the free energy barriers, $\Delta G^{\ddagger}$, that can be deduced from the experimental k_{cat}, with our theoretical potential energy barriers, $\Delta V^{\ddagger}$. As a matter of fact, the experimental rate constant, k_{cat}, is a global constant that cannot be directly attributed to any particular reaction step. However, to make such a comparison we calculated the $\Delta G^{\ddagger}$ value that in a one-step process governed by the transition-state theory would lead to a rate constant equal to k_{cat}. From the theoretical point of view the theoretical potential energy barriers are determined by the highest energy point along the QM/MM potential energy profiles. On the other hand, we have to note

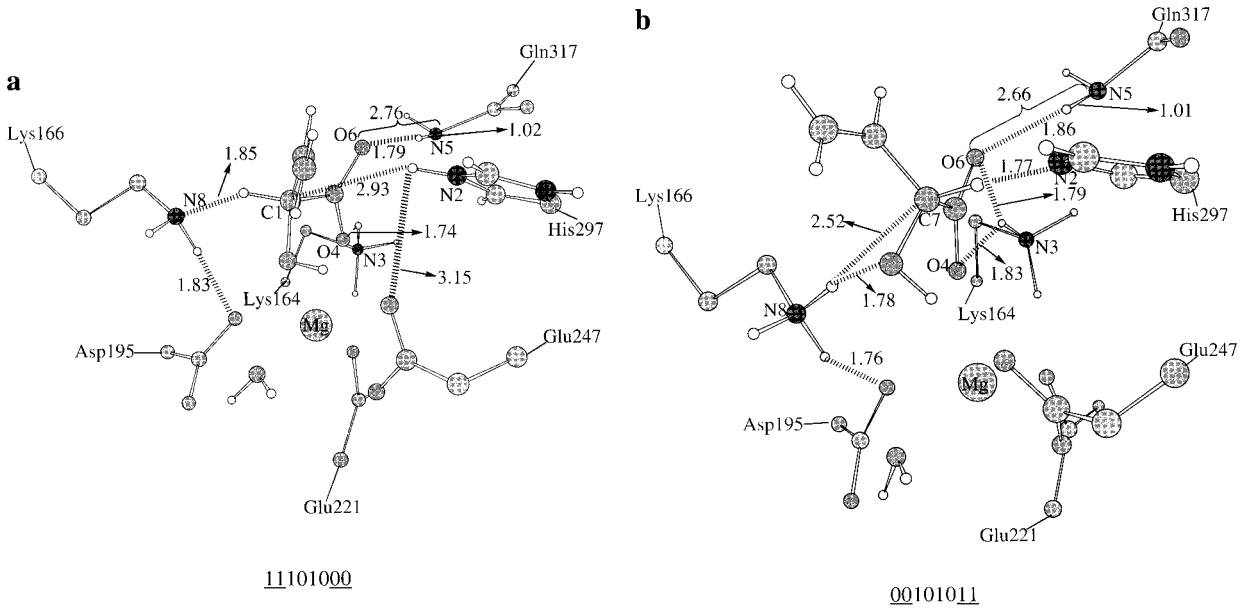

Figure 11. (a) Structure of the active site at the stationary point S_m. The labels used to identify some atoms are the same as in Figure 4. Distances are given in Å. (b) Structure of the active site at the stationary point R_m. The labels used to identify some atoms are the same as in Figure 4. Distances are given in Å.

that our results indicate that the reaction proceeds at least through three different mechanisms, in such a way that the effective potential energy barrier attributed to the overall reaction indeed would be lower than the particular potential energy barriers associated with each mechanism. Thus, the three last columns of Table 6 indicate that in both S-to-R and R-to-S directions mec II and mec III are faster, that is, more favorable than mec I. Despite the approximations used, there is a good qualitative agreement when comparing the experimental free energy barriers of 14.27 and 14.29 kcal/mol for (*S*)- and (*R*)-vinylglycolate, respectively, with the value of the global potential energy maximum of the most favorable mechanisms, that is around 20 kcal/mol and around 18 kcal/mol, for (*S*)- and (*R*)-vinylglycolate, respectively. In addition, the first column of Table 6 indicates that (*S*)-vinylglycolate and (*S*)-mandelate are racemized by MR enzyme at a similar rate. In comparison to these rate values the reaction turns out to be faster with (*R*)-mandelate as substrate but slower when the substrate is (*R*)-vinylglycolate. However, we obtain smaller potential energy barriers for the reaction with (*R*)-vinylglycolate than with (*S*)-vinylglycolate.

The Existence of the Proposed LBHB in the Reaction Catalyzed by MR Enzyme. As mentioned above, the hydrogen bond between the residue Glu317 and the carboxylate oxygen of the substrate has been proposed to be an LBHB.[1] The structures of the stationary points found along mec I, mec II, and mec III that model the anionic intermediate allow theoretical analysis of the features of this hydrogen bond. For all of them, the hydrogen bond distance O5−O6 is short (see Figures 5a, 5b, and 10), but the angle O5−H−O6 is not linear, with values in the range 150−160°. Taking into account that the presence of a very low barrier for proton transfer is the feature that best defines an LBHB and that it is the reason for the name given to this type of hydrogen bond, we have calculated the barrier for proton transfer through this hydrogen bond in one of the calculated anionic intermediates. Among all of the stationary points where the α-carbon has a carbanion character (after abstraction of the α-proton), the stationary point I (Figure 10), that is a dianion, should be the structure with the strongest hydrogen bond. However, in this stationary point the energy barrier for the proton transfer from O5 to O6 is as high as 11.64 kcal/mol. That is, taking into account the definition that we have used in previous studies for the term LBHB,[15,16] we feel capable of saying that it is not an LBHB within our model reaction. In other words, we deduce that the first vibrational wave function, calculated on the multidimensional energy surface, would not have its maximum at the region that corresponds to the transition state of the proton transfer along the hydrogen bond; that is, the high-energy barrier for proton-transfer prevents the delocalization of the bridging proton between O5 and O6.

The Catalytic Role of the Hydrogen Bond between Glu317 and the Substrate. Despite the previous conclusion, we cannot discard the possibility of an important contribution of the mentioned hydrogen bond in the catalysis. To consider this proposal we have done a theoretical study of the racemization of vinylglycolate in the model of the active site of the mutant enzyme E317Q. The mutation affects directly the features of this hydrogen bond and, as a consequence, may provide a good insight into the energetic role of the wild-type hydrogen bond interaction. The geometry optimization of the moving part of the model of the complex mutant enzyme-(*S*)-vinylglycolate leads to the stationary point that is partially represented in Figure 11a and that we have called S_m. The relative position of the enzymatic residues of the model of the mutant enzyme with respect to the (*S*)-vinylglycolate molecule is very similar to the one found in the stationary points S and S2 (Figures 4a and 8, respectively), that model the complex native enzyme-(*S*)-vinylglycolate. This result is in agreement with the experimental observation that there are not conformation alterations that accompany the E317Q substitution in the complex of the enzyme with the (*S*)-atrolactate inhibitor.[2] However, it is worthy to note that, in relation to the His297 location, the structure S_m is closer to the structure S2 (Figure 8) than to the structure S (Figure 4a). That is, as in S2 the distance between the protonated ϵ-nitrogen of His297 and the α-carbon of (*S*)-vinylglycolate is about 2.94 Å, shorter than in S, because in S_m His297 is not interacting by the hydrogen bond with Glu247. On the other hand, the minimization of the QM/MM energy when the substrate of the model is (*R*)-vinylglycolate leads to the stationary point partially represented in Figure 11b (structure

Table 7. Distances (in Å) between Residues, and Charge of the Metal Ion (in au) in the Active Center of the Stationary Points S_m and R_m, and in the X-ray Structure (exp)

	S_m	R_m	exp[a]
Mg−OH	2.33	3.51	2.48
Mg−O4	2.12	2.08	2.54
Mg−O(Asp195)	2.11	2.12	2.36
Mg−O(Glu221)	2.11	2.05	2.07
Mg−O(Glu247)	2.15/2.34	2.15/2.15	2.01
Mg−OHO	2.14	2.16	2.18
qMg	0.88	0.84	−
N3−O4	2.60	2.68	3.00
N5−O6	2.76	2.66	2.86

[a] PDB crystal structure with code number 1DTN.

R_m), that is also very comparable to the structure calculated for the model complex native enzyme-(*R*)-vinylglycolate (Figure 4b). The six first rows of Table 7 show the distances between Mg cation and its six ligands in the stationary points S_m and R_m, in comparison with the experimental distances found by Mitra et al.[2] in the complex of the mutant with (*S*)-atrolactate inhibitor (last column of Table 7). We note that both carboxylic oxygens of Glu247 interact with the cation in the calculated structures, whereas in the structure determined experimentally only one of them participates in this interaction. In general, in comparison with Table 2 which contains the geometrical features of the stationary points that model the complexes formed with the native enzyme, there is less agreement between the experimental and the theoretical distances in Table 7, but this might be a consequence of the fact that the model used for the mutant enzyme is built from the coordinates of the experimental structure of Table 2. The main difference in Table 7 between theoretical and experimental results is the distance found between Mg cation and the OH group of the substrate in the structure R_m. We cannot discard the goodness of our model from this difference, as the experimental structure, where the inhibitor configuration is S, is not directly comparable with the calculated structure R_m, where the substrate configuration is R. As in the case of the wild-type enzyme, there is not any resolved structure of the mutant E317Q bound with the substrate or an analogue in the R configuration. The comparison between the seventh rows of Tables 2 and 7 indicates that within our model the ESP charge calculated for the Mg in the active site is not very affected by the mutation. However, the main change that occurs on mutation is the lengthening of the distance N5−O6 (Table 7) in both S_m and R_m and in the experimental structure, with respect to the distance O5−O6 (Table 2) in the corresponding structures of the native enzyme. That is, as it has been found experimentally, our results indicate that the mutation mainly affects the features of the hydrogen bond between the residue 317 and the substrate.

Let us now analyze the consequences of the mutation in the calculated reaction mechanisms. The changes between positions 5 and 6 have strong consequences: only one of the three mechanisms found in the active center of the native enzyme, that is mec I, is able to interconvert structures S_m and R_m, via the catalytic proton transfer between positions 3 and 4. Figure 12 represents the energy profile for mec I in the active center of the mutant and Table 8 contains the geometric features and energies of the stationary points found along this mechanism. If we compare the energy profiles in Figures 6 and 12, that correspond to mec I in the active center of the native enzyme model and the mutant enzyme model, respectively, it is clear that they are qualitatively very comparable. The main difference is that mec I in the active center of the mutant enzyme model passes through five steps instead of the six that are required for this mechanism in the active center of the native enzyme. Steps 1 and 5 that lead to the neutral intermediate $I1_m$ and to the product R_m, respectively, correspond to the catalytic proton transfer between positions 3 and 4. Steps 2 and 4 are properly the reactive proton transfers, analogous to steps 2 and 5 of Figure 6. However, the comparison between the distances C7−H in the fifth rows of Tables 3 and 8 indicates that His297 is closer to the α-carbon in $I2_m$ than in I2, and the analysis of the structure of these stationary points shows that the hydrogen bond found between His297 and Glu247 in I2 (Figure 5a) does not exist in $I2_m$ (this difference probably comes from the same difference mentioned above between S and S_m). That is, if we want to do an analogy between the anionic intermediates with code 01011001 found along mec I in the active center of the native enzyme (I2, I3, and I4) and the ones with the same code found along mec I in the active center of the mutant ($I2_m$ and $I3_m$), we conclude that $I2_m$ is more comparable to I3 than to I2. For this reason, in the active center of the mutant the approach of His297 to the α-carbon implies only one step (step 3), along which the configuration change of the α-carbon takes place (the change from C1 to C7 in our code). This step passes through the absolute maximum of the mechanism, with an energy value of 27.44 kcal/mol, higher than the global maximum of mec I in the active center of the native enzyme model in the S-to-R direction (Table 6).

On the other hand, the mechanism that we have called mec II, that proceeds via the catalytic proton transfer between positions 5 and 6, and that is feasible in the active center of the model of the native enzyme, it is not possible in the active center of the mutant. The substitution of the carboxylic group of residue Glu317 ($pK_a \approx 6$) for a carboxamide group that leads to a Gln residue ($pK_a \approx 15$) implies that residue 317 is not acid enough

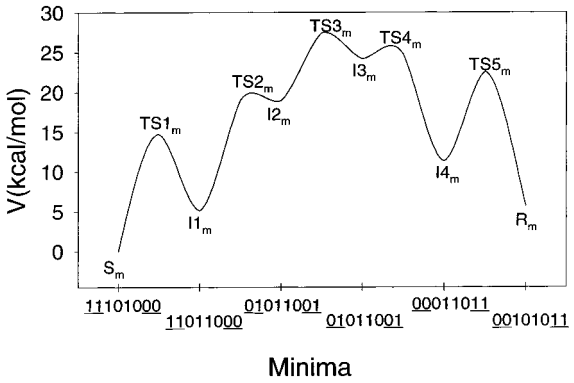

Figure 12. QM/MM potential energy profile of mec I in the active center of the model of the mutant E317Q. The numbers below the *x*-axis follow the code explained in the text to identify the different minimum energy structures found along the mechanism.

Table 8. Distances (in Å) between the Protons and the Heavy Atoms that Participate in Proton-Transfer Processes in the Different Stationary Points Found along Mec I and Potential Energy of Each Stationary Point, in the Case of the Model of the Mutant E317Q.

	C1−H	N8−H	C7−H	N2−H	*V* (kcal/mol)
S_m (11101000)	1.15	1.85	2.93	1.00	0.00
$TS1_m$	1.15	1.82	3.00	1.00	14.71
$I1_m$ (10011000)	1.16	1.80	3.12	1.00	5.13
$TS2_m$	1.57	1.13	3.08	1.00	19.01
$I2_m$ (01011001)	1.61	1.11	3.06	1.00	18.94
$TS3_m$	2.07	1.03	1.73	1.07	27.44
$I3_m$ (01011001)	2.47	1.03	1.63	1.10	24.19
$TS4_m$	2.51	1.03	1.50	1.20	24.80
$I4_m$ (00011011)	2.55	1.03	1.18	1.75	11.34
$TS5_m$	2.52	1.03	1.17	1.76	22.56
R_m (00101011)	2.52	1.03	1.17	1.77	5.66

to deliver a proton to the substrate. That is, the mutation reduces the catalytic role of the hydrogen bond formed between residue 317 and the substrate. In addition, we have not found a dianionic intermediate, analogous to the one found along mec III in the active center of the native enzyme, I (Figure 10), that is stable in the active center of the model of the mutant enzyme. Neither the α-proton abstraction by Lys166 from the stationary point S_m, nor the α-proton abstraction by His297 from R_m, leads to a dianionic intermediate. Taking into account that, as above-mentioned, S_m is geometrically closer to S2 than S, and that the α-proton abstraction from S2 leads to a dianionic intermediate in the active center of the native enzyme, we conclude that the analogue intermediate in the model of the E317Q does not exist. The intermediate I (Figure 10) is stabilized in the active center of the native enzyme as a consequence of different contributions (Mg cation, hydrogen bond O4-Lys164, ion-pair interaction with the protonated His297, ...), among them, the stabilization effect of the hydrogen bond between O5 and O6. Moreover, in going from the anionic structure S2 to the dianionic structure I this hydrogen bond becomes stronger because of the increase of the negative charge on O6. Thus, taking into account that the mutation implies a unique change in the system, that is the substitution of a carboxylate group for a carboxamide group, together with the fact that this change results in a longer distance between the heavy atoms participating in the mutated hydrogen bond, we conclude that, after mutation, the hydrogen bond between positions 5 and 6 is not strong enough to significantly contribute to the stability of the dianionic intermediate.

To summarize, our results indicate that the substitution at position 5 of an oxygen for a nitrogen makes not feasible two of the three mechanisms found (precisely the most favorable ones). That is, in agreement with the experimental results, they suggest that the reaction will be slower in the active center of the mutant E317Q. The first row of Table 6 indicates that the racemization of (*S*)-vinylglycolate to (*R*)-vinylglycolate proceeds mainly through mec II and mec III, whose global maxima have potential energy heights of about 20 kcal/mol, whereas the same reaction in the active center of the mutant enzyme has a global potential energy maximum of 27.44 kcal/mol, that corresponds to the unique feasible mechanism (mec I). In agreement with the experimental measurements the reaction rate reduction is smaller in the R-to-S direction: the global maxima of the most favorable mechanisms in the active center of the native enzyme have energy values around 18 kcal/mol (third row of Table 6), whereas the global potential energy maximum of the reaction in the mutant enzyme model, taking R_m as zero of energies, becomes 21.78 kcal/mol.

Conclusions

In this paper we have performed a quantum mechanical/molecular mechanics (QM/MM) study of the racemization of vinylglycolate catalyzed by the enzyme mandelate racemase. From the observation of the thermodynamics of the reaction (reactant and product) the whole racemization seems to be very simple and obvious at first glance. The experimentally postulated mechanism to convert (*S*)-vinylglycolate to (*R*)-vinylglycolate consists of a two-step quite symmetric process through a dianionic enolic intermediate: abstraction of the α-proton of vinylglycolate by the ϵ-amino group of Lys166, followed by reprotonation by the conjugate acid of His297. However, our theoretical calculations reveal that a much more elaborate nuclear reorganization takes place. The formation of a dianionic intermediate turns out to be an unfavorable event due to the difficulty of the enzymatic residues to stabilize the high concentration of negative charge on the substrate. Then, we have identified three different reaction mechanisms that avoid any dianionic species (mec I and mec II) or make that stabilization possible (mec III). Mec I and mec II involve six steps through six transition states and five intermediates each. Both mechanisms require a proton transfer (the first step) from a residue (Lys164 or Glu317, respectively) to a carboxylic oxygen of vinylglycolate through the corresponding hydrogen bond. That proton transfer precedes the abstraction of the α-proton (the second step) in such a way that the substrate never accumulates more than one negative net charge. Since the previous proton shift has to be reverted during step 6 to yield the product, it can be considered as a real catalytic process itself that allows, in turn, the catalytic action of the enzyme. On the contrary, starting from a structure of (*S*)-vinylglycolate in which the protonated His297 is already quite close to the substrate, a rather asymmetric two-step mechanism (mec III) that takes place through a dianionic intermediate is possible. In this case no previous catalytic proton transfer is required, and the conjugate acid of His297 is now playing a stabilizing role.

From an energetic point of view, the three parallel mechanisms are competitive at room temperature, mec I being slower than the other two. In addition, despite the complexity of the problem and the approximations involved in the calculations, the potential energy barriers theoretically found in this work are qualitatively in good agreement with the experimental free energy barriers determined for racemization of vinylglycolate and mandelate.

In the case of mutant enzyme E317Q, in which Glu317 has been substituted by Gln317, only mec I, the slower one, is able to produce the racemization. Mec II is not possible because the carboxamide group of glutamine 317, conversely to the carboxylic group of glutamic acid, is not acid enough to deliver a proton to the substrate. Mec III is not feasible either because the dianionic intermediate does not exist in the mutant: despite the proximity to the substrate of the protonated His297, now the hydrogen bond between the substrate and Gln317 is not strong enough to stabilize the dianionic structure. As a consequence, the racemization is significantly slowed, in good agreement with the experimental results. The effect of the mutation in the kinetics demonstrates the important role of the hydrogen bond formed by Glu317 in the native enzyme during the catalytic process. However, this hydrogen bond is not a low-barrier hydrogen bond. The hydrogen bond involving Glu317 is important because: (a) glutamic acid is acid enough to allow a proton transfer to the substrate along the hydrogen bond, thus leading to mec II; (b) as the substrate is converted to a dianionic structure due to the abstraction of the α-proton, this hydrogen bond becomes stronger since the electrostatic interaction grows, this way contributing, along with other residues, to make possible mec III. The conclusion that a catalytically important hydrogen bond does not satisfy the conditions for an LBHB has also been reached by other authors.[47]

Our theoretical results for the racemization catalized by mandelate racemase corroborate several relevant points that are known to be general for a wide range of enzymatic reactions: (1) The enzymatic reaction can be the result of several parallel and kinetically competitive channels, in such a way that all them contribute to the global kinetics experimentally measured. (2) Different mechanistic channels can start from different quasi-degenerate structures of the substrate−enzyme complex. (3) The detailed mechanisms often consist of a set of proton transfers

(47) Mulholland, A. J.; Lyne, P. D.; Karplus, M. *J. Am. Chem. Soc.* **2000**, *122*, 534.

among the residues and the substrate: some of them are strictly necessary for the advance of the reaction in the thermodynamic sense, but others must reverse to reach the product, in such a way that they can be considered as catalytic motions that make possible the enzymatic catalysis. (4) The successive proton transfers can lead to charged intermediates that only are accessible if they are stabilized enough; enzymes reach this stabilization by means of other proton transfers, forming strong hydrogen bonds (not necessarily low-barrier hydrogen bonds) or approaching the suitable residues to the substrate.

Finally, some methodological aspects should be mentioned. According to the variational transition-state theory,[48,49] the rate constant depends on the generalized free energy barrier, that is, the maximum value of the generalized free energies associated with a set of dividing surfaces built up along a suitable reaction path taken as a reference. The generalized free energies can be obtained, for instance, from free energy perturbation calculations. The reference path can be a more or less accurate minimum energy path or a distinguished coordinate path as a function of an adequate internal coordinate that connects reactant and product in a reasonable way. The choice of the reference path can be apparently evident, but an exploration of the potential energy surface to locate the set of stationary points that appear along the reaction path is necessary. The racemization catalyzed by mandelate racemase is a clear example of an apparently simple process that actually turns out to be quite more complicated, involving several possible channels with multiple steps, then leading to a priori unexpected reaction paths. Once these reaction paths are determined, the free energy calculations become possible. Additional theoretical work in this direction is now in progress in our laboratory. Anyway, we think that the results presented in this paper, based on potential energy calculations, already shed light on the mandelate racemase mechanism, helping to explain the existing experimental results.

Acknowledgment. We thank Dr. Gerald Monard for the advice and help offered during the realization of this research work. Molecular graphics images were produced using the MidasPlus package from the Computer Graphics Laboratory, University of California, San Francisco (supported by NIH P41 RR-01081).We also are grateful for financial support from DGESIC through Project No. PB98-0915, and the use of the computational facilities of the CESCA and CEPBA coordinated by the C^4 are gratefully acknowledged.

JA002879O

(48) Truhlar, D. G.; Isaacson, A. D.; Garrett, B. C. In *Theory of Chemical Reaction Dynamics*; Baer, M.. Ed.; CRC: Boca Raton, FL, 1985; Vol. IV, p 65.

(49) Truhlar, D. G.; Gordon, M. S. *Science* **1990**, *249*, 491.